Acta Crystallographica Section D
Biological Crystallography
ISSN 0907-4449

How do the X-ray structure and the NMR structure of FMN-binding protein differ?

Kyoko Suto,[a] Kazuhiro Kawagoe,[a] Naoki Shibata,[a] Yukio Morimoto,[a] Yoshiki Higuchi,[a]† Masaya Kitamura,[b] Tadao Nakaya[b] and Noritake Yasuoka[a]*

[a]Department of Life Science, Faculty of Science, Himeji Institute of Technology, 3-2-1 Kouto, Kamigori Ako-gun, Hyogo 678-1297, Japan, and [b]Department of Bioapplied Chemistry, Faculty of Engineering, Osaka City University, Sumiyosi-ku, Osaka 558-8585, Japan

† Present address: Division of Chemistry, Graduate School of Science, Kyoto University, Sakyo, Kyoto 606-8502, Japan.

Correspondence e-mail: yasuoka@sci.himeji-tech.ac.jp

The crystal structure of FMN-binding protein (FMN-bp) from *Desulfovibrio vulgaris* Miyazaki F was solved by the multiple isomorphous replacement method and refined to an R factor of 15.1% at 1.3 Å resolution. FMN-bp exists in a dimeric form in the crystal, in contrast to the monomeric structure determined by NMR. R.m.s. deviations between the crystal structure and the solution structure are more than 2 Å, which implies significant differences. There are some hydrophobic residues in the interface between the two monomers. In particular, Leu122 in the C-terminus has a close contact with the *o*-xylene moiety of FMN, while solvent molecules may cover the *o*-xylene moiety in the solution structure.

Received 27 October 1999
Accepted 5 January 2000

PDB Reference: FNM-bp, 1flm.

1. Introduction

FMN-bp is composed of 122 amino acids and is the smallest of the known proteins which bind FMN (Kitamura *et al.*, 1994). The function of FMN-bp *in vivo* is still unclear, but it may take part in the electron-transfer pathway. A structural study of FMN-bp as a monomer in solution by nuclear magnetic resonance spectroscopy has previously been reported (Liepinsh *et al.*, 1997, 1998). It is suggested that FMN-bp has a structural relationship to the C-terminal domain of chymotrypsin. Subsequently, another possibility was noticed: a structural relationship between FMN-bp and the FAD-binding domain of ferredoxin reductase (Murzin, 1998). We have carried out an X-ray structure analysis at rather high resolution with synchrotron radiation and have found the molecule to exist in the dimeric form. Here, we mainly report the differences between the crystal structure and the solution structure.

2. Experimental and structure determination

FMN-bp was purified as described previously (Kitamura *et al.*, 1994). The protein solution subjected to crystallization contained 15 mg ml^{-1} FMN-bp, 0.1 *M* Tris–HCl pH 8.0 and 200 m*M* sodium chloride, in which FMN-bp is oxidized. Single crystals were grown using polyethylene glycol by the vapor-diffusion method with the micro-seeding technique. The reservoir contained 0.1 *M* buffer solution (MES pH 6.5 or Tris–HCl pH 7.5), 20%(*w*/*v*) polyethylene glycol 6000 or 8000, 0.2 *M* sodium acetate and 20% glycerol (Suto *et al.*, 1999).

The diffraction intensity data of native crystals were collected using synchrotron radiation at beamlines BL-6A and BL-18B at the Photon Factory, KEK, Japan (Table 1). The programs *DENZO* and *SCALEPACK* (Otwinowski & Minor, 1997) were used for data processing. For the individual data sets, the overall $R_{\rm merge}$ was in the range 2.6–4.8% and $R_{\rm merge}$ for the highest shell was less than 20% with $I \geq \sigma(I)$. All crystals belong to the monoclinic space group $P2_1$, with unit-cell parameters a = 37.22 (3), b = 84.59 (5), c = 41.10 (2) Å, β = 94.07 (5)°. Assuming that two molecules are present in the asymmetric unit, their $V_{\rm m}$ values are within the range 2.35–2.36 Å^3 Da^{-1}, which is reasonable for protein crystals.

Although molecular replacement using *X-PLOR* was attempted with the structures obtained by NMR methods, no likely solutions were found. Consequently, the structure was solved by multiple isomorphous replacement. Three derivatives were prepared. Crystals were soaked in solutions containing K_2PtCl_6, K_2IrCl_6 or $UO_2(NO_3)_2$. The data from the derivative soaked in K_2PtCl_6 solution were collected using synchrotron radiation at the BL-6A beamline and the data from the other derivatives were collected using Cu $K\alpha$ X-rays on a MacScience DIP3000 imaging plate. The data processing was carried out in a similar way to that used for the native data. Heavy-atom positions were determined by difference Patterson map from native 1 using *XTAL-VIEW* (McRee, 1993). Phase calculation and refinement of heavy-atom positions were carried out using *MLPHARE* (Collaborative

Table 1
Data collection and phasing statistics.

	Native 1	Native 2	K_2PtCl_6	K_2IrCl_6	$UO_2(NO_3)_2$
Data-collection statistics					
Resolution range (Å)	30.0–1.60	30.0–1.20	40.0–2.30	40.0–2.30	40.0–2.20
Number of measurements	112414	337547	43305	23348	27423
Number of reflections	22986	68514	10213	10591	11083
Completeness	68.7	86.6	89.8	92.7	85.7
R_{merge} (%)	4.8	2.6	8.7	6.2	7.9
$I/\sigma(I)$†	31.9 (4.1)	28.9 (2.0)	15.6 (4.9)	17.5 (5.6)	13.6 (4.6)
Phasing statistics					
Phasing power‡ (centric/acentric)			1.54/1.56	0.82/0.85	0.97/1.0
Cullis R factor§ (centric/acentric)			0.59/0.73	0.78/0.88	0.74/0.82

† Highest resolution shell ‡ R.m.s. isomorphous difference divided by the r.m.s. residual lack of closure. § Cullis R factor = $\sum \big| |F_{PH}| \pm |F_P| - |F_H(\text{calc})| \big| / \sum |F_{PH}| \pm |F_P| \big|$.

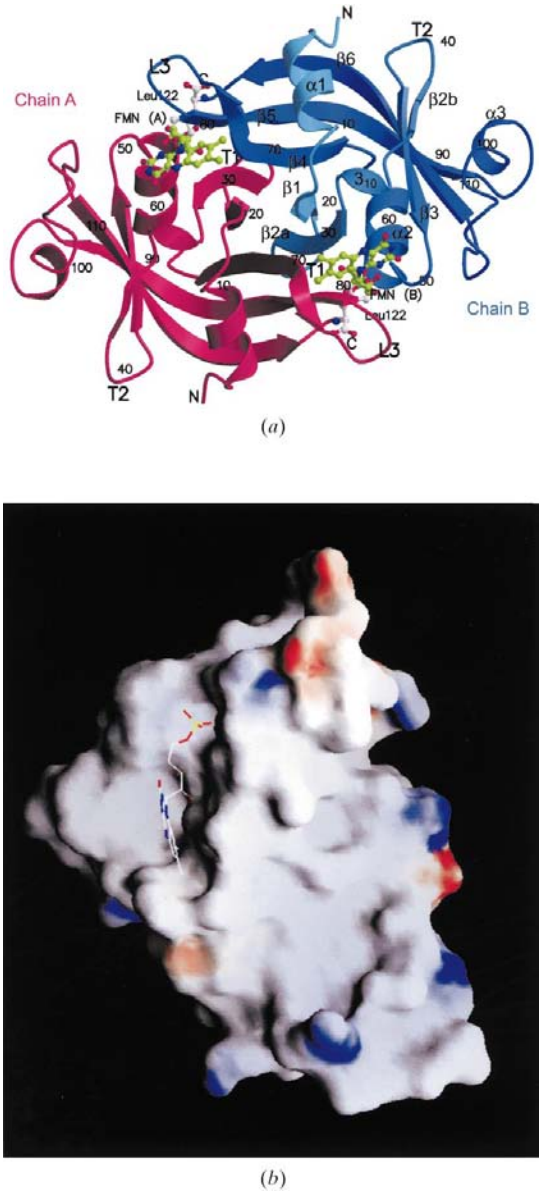

(*a*)

(*b*)

Figure 1
(*a*) A schematic diagram of dimeric FMN-bp. Two chains, chain *A* and chain *B*, are shown as red and blue models, respectively. Only Leu122s and FMNs are depicted as ball-and-stick models. (*b*) Molecular interface. The charge is illustrated by the color, red being acidic and blue being basic. FMN is superimposed as a wire model.

Computational Project, Number 4, 1994), followed by solvent flattening and histogram mapping using *DM* (Cowtan, 1994). Some parts of molecules could be located in the electron-density map. A non-crystallographic symmetry (NCS) matrix was calculated from the partial model, because NCS could not be defined clearly from the self-rotation function using *X-PLOR* (Brünger, 1993) and *CCP*4. The whole model was built after the map had been improved with successive solvent flattening, histogram mapping and NCS averaging. Refinement was carried out using *X-PLOR* against native 1 with NCS restraints to the resolution limit 2.0 Å and using *SHELX*97 (Sheldrick & Schneider, 1997) against native 2 to 1.30 Å. The final R_{work} was 15.0% and R_{free} was 18.2% for native 2 in the resolution range 8.0–1.30 Å. The Ramachandran plot of FMN-bp shows that the percentage of residues with (φ, ψ) conformational angles in the most favoured region is 93.1% (188 residues) and that all remaining residues (6.9%, 14 residues) are in additional allowed regions. The four terminal residues, ten proline and 28 glycine residues were excluded from these calculations. R.m.s. deviations and distances were calculated using *X-PLOR* and *LSQKAB* (Collaborative Computational Project, Number 4, 1994). Figures were drawn using *MOLSCRIPT* (Kraulis, 1991) and *RASTER3D* (Merrit & Murphy, 1991). The accessible surface area was calculated with *GRASP* (Nicholls *et al.*, 1991).

3. Results and discussion

3.1. Overall structure

There are two FMN-bp molecules in the asymmetric unit. They are related by a non-crystallographic twofold axis and are considered to form a dimer as shown in Fig. 1(*a*). We designate the two molecules as molecule *A* and molecule *B*; the amino-acid residues or cofactors belonging to each molecule are distinguished with superscripts (for example, ^{A}Phe104) when necessary. The r.m.s. deviation of main-chain atoms between the two molecules is no more than 0.16 Å with an average *B* factor of 14.4 Å^2, which indicates that the two molecules are almost identical. The secondary structure consists of seven β-strands, three α-helices and a short 3_{10} helix as follows: residues 1–215(β1), 26–32 (β2a), 37–39 (β2b), 43–48 (β3), 63–74 (β4), 79–92 (β5), 109–120(β6), 4–10 (α1), 34–35 (3_{10}), 52–60 (α2), 96–99 (α3). In addition, two turns and a loop are assigned as follows: residues 22–25 (T1), 39–42 (T2) and 75–78 (L3).

The molecular interface is flat and mainly hydrophobic (see Fig. 1*b*); Ala17, Ala19, Pro26, Leu28, Leu65 and Leu84 take part in the association of the two monomers. In addition, many hydrogen bonds are formed in the peripheral part of the interface. ^{A}Glu21 O$^\varepsilon$ is bonded to ^{B}Gln21 N$^\varepsilon$, ^{A}Asn30 N$^\delta$ is bonded to ^{A}Thr67 O$^\gamma$ and the two ^{A}Arg63 NH2 atoms are bonded to ^{B}Asp24 O, where molecules *A* and *B* can interchange. Thus, the association of the two molecules into the dimer involves hydrophobic interactions in the central part as well as the hydrophilic interactions surrounding them. The contacting area seems to be significantly broad. The accessible surface area of an FMN-bp monomer is calculated to be 6500 Å^2 per molecule. In the case of the dimer, the accessible surface area is 10 200 Å^2. Therefore, an area of 1400 Å^2 is lost on dimerization. The molecular weight was estimated to be 17 500 Da by the gel-filtration method; this was higher than that calculated for the monomer (Kitamura *et al.*, 1994). This suggests that FMN-bp at least partially exists as a dimer in solution.

The cofactor FMN is situated in the groove near the interface and is held in place by hydrophobic and hydrophilic interactions (Fig. 2*a*). The numbering scheme in the FMN molecule is the same as

that used in the Protein Data Bank. The distance between the C(7) atoms of FMNs is 16.9 Å, which suggests that there is no significant interaction between them. A ribityl phosphate moiety is held in place by hydrogen bonds to the side-chain atoms of His27 and Thr54, the main-chain atoms of Lys53 and Thr54, and three water molecules. The atoms in the 2,4-pyrimidinedione (uracil) moiety are bound tightly by hydrogen bonds to surrounding residues; for example, the O(2) atom to the main-chain N atoms of Gly49 and Gly50, the N(3) atom to the main-chain O atom of Pro47 and the O(4) atom to Thr31 $O^{\gamma 1}$ with a distance of 2.78 Å. The N(1) atom of the 2,4-pyrimidinedione moiety forms a hydrogen bond with the O(4)* atom of the ribityl side chain in FMN. An *o*-xylene moiety of FMN is located near Trp32 and Val115. It is noteworthy that Leu122 in the pairing molecule also shows hydrophobic interactions. These three residues contacting the *o*-xylene moiety form a hydrophobic core. The loop Gly75–Pro79 seems to cover this hydrophobic core. At the back of the 2,4-pyrimidinedione moiety of FMN, the side chain of Met51 runs parallel with the ribityl side chain towards the 2,4-pyrimidinedione moiety, in contrast to the case in most flavoproteins, where the methionine side chain is found below the *o*-xylene moiety. This difference suggests that Met51 is indispensable for the activity of FMN-bp and might be responsible for the difference in redox potential between FMN-bp and other flavoproteins (Druhan & Swenson, 1998).

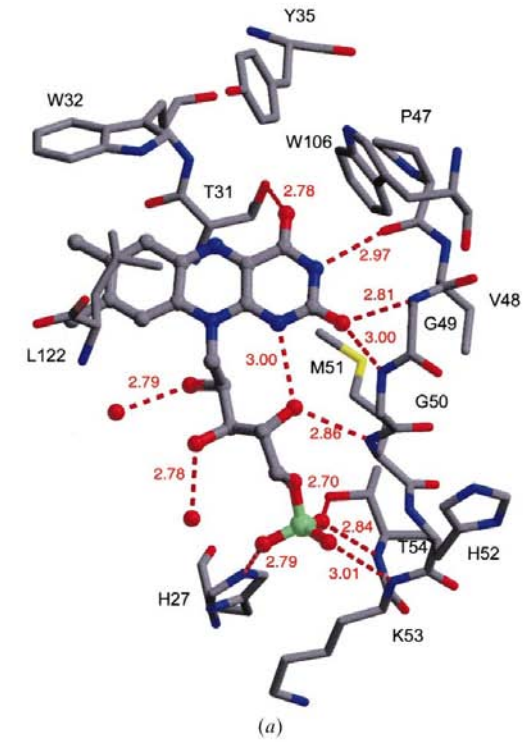

Figure 2
(*a*) Stick models showing residues around FMN. Hydrogen bonds are shown as red broken lines, with distances in Å. Only the Leu122 residue belongs to molecule *B*; the others belong to molecule *A*. (*b*) Pocket of FMN-binding site. FMN is drawn in orange. Aromatic side chains are drawn in yellow, and cationic side chains are in cyan. Some of the aromatic side chains (Trp32, Tyr35 and Trp106) are exposed to solvent.

In the crystal structure, FMN lies at the bottom of the hydrophobic pocket (Fig. 2*b*). It is interesting to note that there are some exposed aromatic residues at the back of the pocket. Tyr35, Trp106 and Phe104 are exposed to the solvent regions and may participate in the electron transfer. Tyr35 and Phe104 are located within interacting distance. The side chain of Lys105 is pointing into the solvent and may play a role in the recognition of a target protein to which an electron is transferred.

3.2. Comparison of the crystal structure with the solution structure

The most remarkable feature of the X-ray structure is that FMN-bp forms a dimer, in contrast to the structure deduced from NMR spectroscopy in which there was no consideration of the possibility of a dimeric form. 20 sets of coordinates of the NMR structure have been deposited in the Protein Data Bank with the accession code 1axj (Liepinsh *et al.*, 1997, 1998). The r.m.s. deviation of main-chain atoms in each structure from the average structure is no more than 0.54 Å, which is low considering the number of residues (Fig. 3*a*). On the other hand, the r.m.s. deviation of the main-chain atoms of the X-ray structure from the average NMR structure is as much as 2 Å, which suggests significant discrepancies are observed between the two structures. The deviations between corresponding atoms in the main chains of the two structures are also plotted against the amino-acid sequence. The monomeric NMR structure is superimposed on the dimeric X-ray structure in Fig. 3(*b*). It is clear that the conformations of the residues around Asn77, forming L3, have the most remarkable differences. A large discrepancy between the X-ray and NMR structures is also observed in the vicinity of the C-terminal region and is compared in Fig. 3(*c*). In the X-ray structure, as described before, ^{A}Leu122 is located near the *o*-xylene moiety of ^{B}FMN. This hydrophobic part is covered by the reverse turn formed by residues ^{A}Gly75, ^{A}Arg76, ^{A}Asn77 and ^{A}Gly78. In contrast, the hydrophobic side chain of Leu122 is buried under the hydrogen-bond network among the side chains of ^{A}Arg76, ^{A}Asn77 and the main-chain atoms of ^{A}Leu122, ^{A}Gly80 *etc*. in the NMR structure. This discrepancy might arise from the fact that FMN-bp forms a dimer in the crystal, whereas it is postulated to exist as a monomer in solution where the NMR experiment was carried out.

As described, the *o*-xylene moiety of FMN interacts with Leu122 of the pairing molecule and is therefore not exposed to solvent in the X-ray structure. The solvent-accessible surface area of FMN calculated for the dimeric form is 13%, in agreement with other flavoproteins, although it was 34% for the NMR structure. The lower accessibility of FMN in the crystal seems to be natural, as a rather low dissociation constant of 0.43 n*M* (unpublished data) is observed. In addition, the hydrophobicity around FMN, particularly around the *o*-xylene moiety, seems to play an important role in the oxidative and reductive beha-

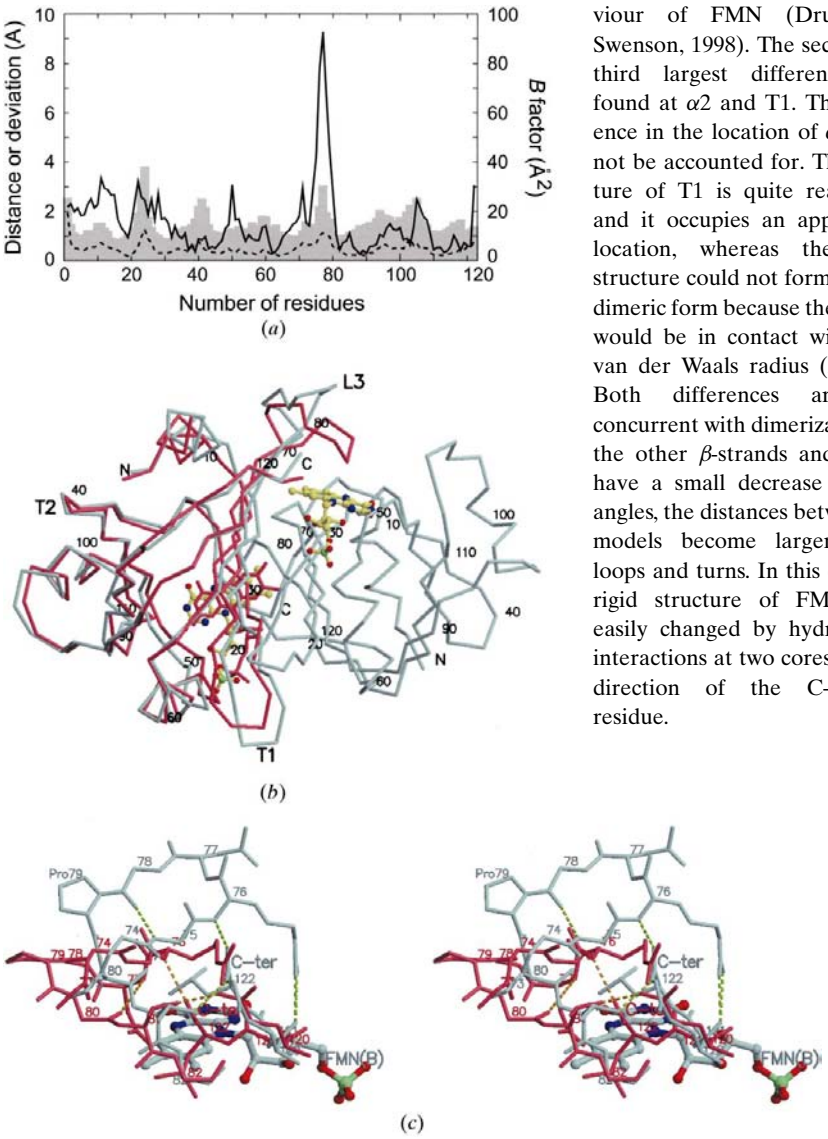

Figure 3
(*a*) Backbone r.m.s. differences between dimeric FMN-bp from X-ray and monomeric FMN-bp from NMR. The solid line indicates distance between the dimer and the averaged monomer calculated from the 20 conformers deduced by NMR. The dotted line indicates the r.m.s. deviations of 20 conformers from the averaged structure for each residue. Histograms show temperature factors in the X-ray structure. (*b*) Superposition of C^{α} models of the X-ray dimer structure and the NMR monomer structure. The averaged NMR structure (red) is superposed on chain *A* from the X-ray structure (blue). In case of the dimer, FMN is near the C-terminal. (*c*) The most different point in (*b*). L3 and C-terminal residues are shown. In addition, FMN is near them in the X-ray structure.

viour of FMN (Druhan & Swenson, 1998). The second and third largest differences are found at α2 and T1. The difference in the location of α1 could not be accounted for. The structure of T1 is quite reasonable and it occupies an appropriate location, whereas the NMR structure could not form a stable dimeric form because the T1 part would be in contact within the van der Waals radius (Fig. 3*b*). Both differences are also concurrent with dimerization. As the other β-strands and helices have a small decrease in their angles, the distances between the models become larger in all loops and turns. In this case, the rigid structure of FMN-bp is easily changed by hydrophobic interactions at two cores and the direction of the C-terminal residue.

We would like to thank Drs N. Sakabe, N. Watanabe and M. Suzuki of the Photon Factory for their kind help in intensity data collection and processing, which were performed under the approval of the Photon Factory (proposal No. 98G175). This work is partly supported by Monbusho (Grant-in-Aid for Encouragement of Young Scientists, No. 11780474 to NS). YM and NY are members of the Sakabe Project of TARA.

References

Brünger, A. T. (1993). *X-PLOR Version 3.1 Manual.* New Haven, Connecticut, USA: Yale University Press.
Collaborative Computational Project, Number 4 (1994). *Acta Cryst.* D**50**, 760–763.
Cowtan, K. (1994). *Jnt CCP4/ESF–EACBM Newslett. Protein Crystallogr.* **31**, 34–38.
Druhan, L. J. & Swenson, R. P. (1998). *Biochemistry*, **37**, 9668–9678.
Kitamura, M., Kojima, S., Ogasawara, K., Nakaya, T., Sagara, T., Niki, K., Miura, K., Akutsu, H. & Kumagai, I. (1994). *J. Biol. Chem.* **269**, 5566–5573.
Kraulis, P. J. (1991). *J. Appl. Cryst.* **24**, 946–950.
Liepinsh, E., Kitamura, M., Murakami, T., Nakaya, T. & Otting, G. (1997). *Nature Struct. Biol.* **4**, 975–979.
Liepinsh, E., Kitamura, M., Murakami, T., Nakaya, T. & Otting, G. (1998). *Nature Struct. Biol.* **5**, 102–103.
McRee, D. E. (1993). *Practical Protein Crystallography*. San Diego: Academic Press.
Merrit, E. A. & Murphy, M. E. (1991). *Acta Cryst.* D**50**, 869–873.
Murzin, A. G. (1998). *Nature Struct. Biol.* **5**, 101.
Nicholls, A., Sharp, K. A. & Honig, B. (1991). *Proteins Struct. Funct. Genet.* **11**, 281–296.
Otwinowski, Z. & Minor, W. (1997). *Methods Enzymol.* **276**, 307–326.
Sheldrick, G. & Schneider, T. (1997). *Methods Enzymol.* **277**, 319–343.
Suto, K., Kawagoe, K., Shibata, N., Morimoto, Y., Higuchi, Y., Kitamura, M., Nakaya, & Yasuoka, N. (1999). *Acta Cryst.* D**55**, 1089–1090.